Biomedical Physics & Engineering Express

ENDORSED BY IPEM Institute of Physics and Engineering in Medicine

PAPER • OPEN ACCESS

Submicron infrared imaging of an oesophageal cancer cell with chemical specificity using an IR-FEL

To cite this article: J Ingham *et al* 2018 *Biomed. Phys. Eng. Express* **5** 015009

Biomedical Physics & Engineering Express

PAPER

Submicron infrared imaging of an oesophageal cancer cell with chemical specificity using an IR-FEL

J Ingham[1], T Craig[1], C I Smith[1], A Varro[2], D M Pritchard[2], S D Barrett[1], D S Martin[1], P Harrison[1], P Unsworth[1], J D Kumar[2], A Wolski[1,3], A Cricenti[4], M Luce[4], M Surman[3,5], Y M Saveliev[3,5], P Weightman[1] and M R F Siggel-King[1,3,5]

[1] Department of Physics, Oliver Lodge Laboratory, University of Liverpool, Liverpool, L69 7ZE, United Kingdom
[2] Department of Cellular and Molecular Physiology, Institute of Translational Medicine, University of Liverpool, Liverpool, L69 3GE, United Kingdom
[3] Cockcroft Institute, Sci-Tech Daresbury, Warrington, WA4 4AD, United Kingdom
[4] Istituto di Struttura della Materia, CNR, via del Fosso del Cavaliere 100, Rome, Italy
[5] Accelerator Science and Technology Centre (ASTeC), STFC Daresbury Laboratory, Sci-Tech Daresbury, Warrington, WA4 4AD, United Kingdom

E-mail: michele.siggel-king@stfc.ac.uk

Keywords: cancer, oesophageal, chromosome, infrared, SNOM, FEL, cell

OPEN ACCESS

RECEIVED
17 September 2018

REVISED
11 October 2018

ACCEPTED FOR PUBLICATION
22 October 2018

PUBLISHED
8 November 2018

Abstract

This work reports the use of an infrared spectroscopic version of scanning near-field optical microscopy (IR-SNOM) and shows that it is possible to reveal subcellular entities via their chemical constituents in a label-free human oesophageal adenocarcinoma cell (OE33). This work presents the first high spatial resolution (~0.15 μm) study of features imaged at various wavelengths within a cancer cell. The clear illumination of sub-micron sized moieties within a cell is a major step forward and is a key requirement for understanding cancer and for the study of other diseases and healthy tissue. The stable and tuneable light source was provided by the infrared free electron laser on the ALICE accelerator at Daresbury. The images reveal a structure with a size and wavelength absorption that are consistent with a chromosome and open the possibility of observing other localized structures, such as microvesicles, that play an important role in the development and spread of cancers.

1. Introduction

There is considerable interest in the development of label-free imaging techniques that provide chemical information with high spatial resolution. Such techniques find application in a wide variety of fields including material science and nanotechnology but they are of particular interest in the biological and medical sciences. The latter fields have benefitted in recent years from the development of super resolution imaging techniques that operate in the visible region of the electromagnetic spectrum and overcome the diffraction limit by the use of a variety of fluorescent proteins that are used to label particular features of interest in biological systems [1, 2]. Infrared (IR) techniques have the advantage over experiments in the visible region of the spectrum in that they can provide chemical signatures of molecules without the need to insert active elements into the specimen. For this reason there has been considerable progress in the development of IR imaging techniques to provide insight into biomedical processes and in particular to provide cost-effective and accurate diagnostics for a range of cancers [3]. Of the IR imaging techniques, Fourier transform infrared (FTIR) imaging [4] is the most commonly used in the study of cancer. Despite its high spectral resolution, the spatial resolution that can be obtained over the wavelength region of this study (5.7–8.1 μm) is limited by diffraction to roughly half of the wavelength. It has been shown that scanning near-field optical microscopy (SNOM) has the potential to provide images with significantly higher spatial resolution [3, 5–9] than those obtained with FTIR. However, in common with all scanning probe techniques, SNOM acquires its data sequentially point-by-point, and hence data acquisition times are inherently longer compared to other IR imaging techniques that use array detectors.

There are a number of approaches to the development of IR-SNOM techniques, each of which has

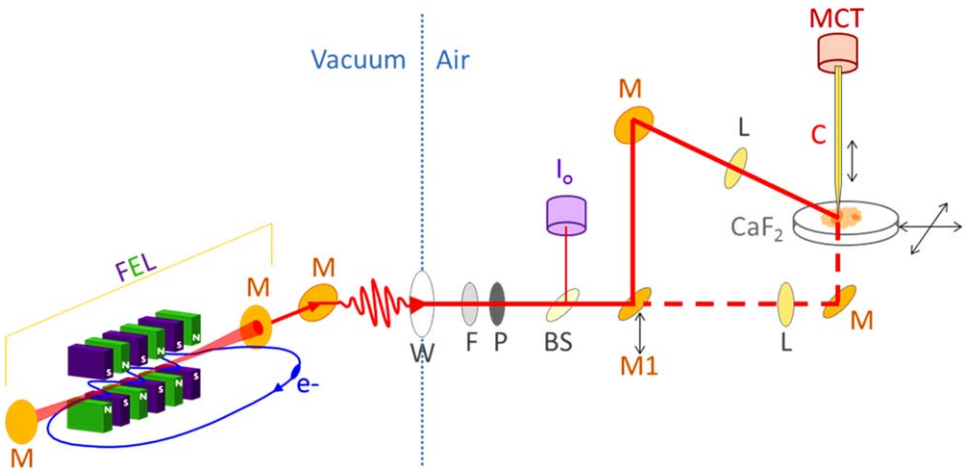

Figure 1. Schematic of the FEL and aperture IR-SNOM end-station set-up. The IR laser pulse was generated in the FEL and exited the evacuated beamline through a KBr window (W). The schematic shows the mirrors (M), lenses (L), beam splitter (BS), polarizer (P), filters (F) and the reference detector (I_o). The sample was mounted onto a CaF_2 slide, which was rastered in the horizontal plane. The chalcogenide fibre (C) moved in the vertical dimension to follow the contours of the surface. The SNOM signal was detected using an MCT detector. The light path for reflection mode is shown by the solid line; the dashed line shows the transmission path. A mirror (M1) can be inserted or removed to select the mode.

strengths and weaknesses, none of which are completely understood [3, 5–14]. The principal SNOM techniques are photothermal imaging, which uses a sharp tip to record changes in the local thermal expansion of a specimen under IR illumination [13, 14], scattering scanning near-field optical microscopy (s-SNOM), which employs a detector phase-locked to an oscillating sharp tip [10–12, 15–18], and aperture SNOM, which collects and detects the light directly under an aperture tip. [6–9]. The first two techniques are able to achieve resolutions of 10's of nm. The commercially available Bruker Anasys nanoIR^{TM} AFM-IR instruments [19] use a sharp tip, together with thermal imaging, to achieve $<$10 nm spatial resolution for chemical imaging and boast monolayer measurement sensitivity. However, the lateral resolution that can be achieved is dependent upon the sample and on biological samples is $\sim$10's of nm. The aperture SNOM is the only SNOM technique so far that has been shown to reveal information on the variation of the chemical composition within a cell and it can do so at lateral resolutions of 100 nm, which is ideal for the study of the larger subcellular features and large molecules. The use of sharp tips and/or a narrow aperture significantly reduces the IR signal collected from the specimen and puts time constraints on the collection of images with acceptable signal-to-noise levels.

In a recent work, high quality IR-SNOM images of a human oesophageal adenocarcinoma cell (OE33) at subcellular spatial resolution were obtained [9] using the highly stabilized IR free-electron laser (IR-FEL) on the ALICE accelerator at Daresbury [20, 21] for experiments in both reflection and transmission SNOM modes. This earlier work compared the IR-SNOM images with images of the same cell obtained using FTIR in order to compare the two techniques. This work reports an analysis of the whole cell images obtained in the previous study [9] and of a set of small high-resolution images taken from within the cell in order to establish the potential of the technique to reveal important information on the detailed chemical structure of cells. The first IR observations of a feature attributed to a human chromosome in a cancer cell and a feature with the expected size of a microvesicle are reported. Changes in chromosomes and the presence and behaviour of microvesicles are currently the focus of considerable research in cancer; the demonstration that this technique has the capability to determine the presence, location and chemical composition of these structures has the potential to make major contributions to research in these and related fields.

2. Experimental

The SNOM data presented in this paper were obtained during the experiments reported earlier [9] using the IR-SNOM installed on the end-station of the IR-FEL beamline at the Accelerators and Lasers In Combined Experiments (ALICE) energy recovery accelerator at the STFC Daresbury Laboratory [20, 21]. The wavelength of light from the FEL could be varied continuously from $\sim$1818 to $\sim$1136 cm^{-1} (5.5–8.8 μm); the bandwidth (FWHM) typically varied from $\sim$23 at 1667 cm^{-1} ($\sim$0.09 at 6.0 μm) to $\sim$20 at 1250 cm^{-1} ($\sim$0.13 at 8.0 μm). The IR-FEL operates at a macro-pulse repetition rate of 10 Hz. The stability of the intensity of the macro-pulses was $\sim$1% when running under optimum conditions [21]. The IR-light from the FEL was transported to the experimental area through an evacuated beamline and exited the beamline through a KBr window. A schematic of the

experimental set-up is shown in figure 1. Higher orders of light from the FEL were filtered out and the light was attenuated using a set of polarizers. A CaF_2 beam-splitter was used to divide the IR-light so that approximately 80% went to the SNOM and 20% was used as a reference signal (I_o). The I_o signal was monitored with a pyroelectric power meter (Gentec-EO, Quebec, Canada) which provided a measure of the relative intensity of each macro-pulse.

The end-station was configured for the standard reflection mode for an IR-SNOM, where the light was focused onto the sample at a grazing incidence angle of approximately 15°. Experiments in transmission mode, where the FEL beam was perpendicular to the plane of the slide and focused through the CaF_2 slide onto the sample, were made possible by removal of a mirror. The SNOM imaging tip was etched onto an IR-transmitting chalcogenide fibre of core diameter 6 μm; the tip was gold-coated [22] to create a small aperture through which the light was collected. The sample was then rastered under the tip using shear-force feedback to keep the tip-to-sample distance constant. The raster scan rate was 10 Hz, which was limited by the repetition rate of the FEL. In both modes the signal was collected by the aperture fibre in the near-field region above the specimen. A liquid nitrogen cooled mercury–cadmium–telluride (MCT) detector was used to detect the IR-light that was transmitted through the fibre. The SNOM was mounted onto an inverted optical microscope, which was used to locate the specific areas of interest on the sample and to position them within the SNOM scan area.

Human Caucasian oesophageal adenocarcinoma cells from an OE33 culture [23] were obtained from HPA Culture Collections (Sigma, Dorset, UK) and maintained and prepared for experiments as previously described [9]. In brief, the cells were cultured at 37 °C in a 5% CO_2 atmosphere in Roswell Park Memorial Institute (RPMI 1640) growth media (Sigma) supplemented with 2 mM glutamine (Sigma), 10% v/v foetal bovine serum (FBS) (Invitrogen, Paisley, UK) and 1% v/v penicillin/streptomycin (Sigma) until they reached 70%–80% confluence. Sterile CaF_2 discs (20 mm diameter × 2 mm thick) were then placed in wells of a tissue culture well plate. The cells (2×10^4 ml^{-1}) were seeded on each disc and incubated in a 5% CO_2 incubator at 37 °C for two days. After two days the media was removed and the cells were fixed with a 4% v/v paraformaldehyde (PFA) (Sigma) solution and stored in 1x phosphate buffered saline solution at 4 °C until required. Prior to imaging, the slide was rinsed with Millipore ultrapure water (18 MΩ cm), the back surface wiped and then left to dry for a minimum of 90 min. The slide was then mounted onto the SNOM.

At each wavelength the topography, raw SNOM intensity and the IR-reference data (I_o) were collected simultaneously. Images of the whole cell were acquired with 110 × 110 pixels and a raster step size setting of 1 μm. High-resolution images of a small region within the cell were acquired with 80 × 80 pixels and a raster step size setting of 0.1 μm. For both sets of images the same scanning tip was used.

Images were collected at a small number of carefully chosen wavenumbers, which correspond to particular contributions to the chemical structure of the cell. The choice of wavelengths was determined from the extensive literature on the results of FTIR studies of proteins, nucleic acids and other biological molecules [24–27]. These studies indicate that the Amide bands are associated with the secondary structure of proteins and that the peak of the Amide I band at ~1650 cm^{-1} predominately reflects the α-helix structure of proteins. There is somewhat weaker evidence for associating a peak at ~1538 cm^{-1} with the β-sheet structure of proteins. Studies of nucleic acids indicate that a peak at 1242 cm^{-1} is associated with a nucleic acid asymmetric phosphate stretch involving DNA and/or RNA [6, 9, 26, 28, 29]. Similarly a wavelength at 1751 cm^{-1} can be attributed to a carbonyl stretch that is mainly associated with lipids. In addition, in order to provide a neutral reference, images were collected at 1370 cm^{-1}. This wavenumber is not dominated by a single chemical moiety although there is a contribution from the CH_3 deformation band of lipids [26, 28]. Images taken at 1370 cm^{-1} roughly follow the topography of the sample. The number of images that could be acquired was limited due to the finite time allocated on the accelerator-based IR-FEL source and the time required to collect each image. To ensure reproducibility, at least two images were obtained for all the results presented in this work.

Various pre-processing techniques were applied to the raw IR-SNOM images [9]. In brief, the images were first normalized for fluctuations in the FEL power by dividing the raw image signal by the I_o image signal. The second step was to correct for the non-linear response of the piezoelectric drives of the x–y stage of the SNOM. Finally multiple IR-SNOM images were co-registered, using the topography images, to take account of small offsets that can occur between scans. Other common image processing techniques, such as median filtering, were used when appropriate to reduce noise levels without compromising image quality.

3. Results and discussion

The potential of IR-SNOM to reveal chemical contrast information within a cell at ~1 μm resolution was demonstrated in an earlier study of the OE33 cancer cell [9]. The instrument makes it possible to obtain IR-SNOM images at a single wavelength over a wide range of areas: large areas at low spatial resolution or smaller regions at higher spatial resolution (~0.15 μm). In this paper we demonstrate the ability of the IR-SNOM

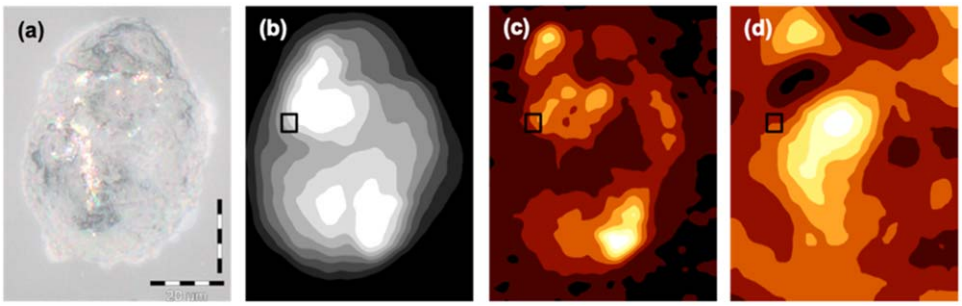

Figure 2. An OE33 cancer cell. (a) Optical microscopy image (400x). Contour plots from (b) topography (SNOM shear-force), (c) IR-SNOM in reflection at 1242 cm^{-1} and (d) IR-SNOM in transmission at 1242 cm^{-1}. The IR-SNOM images are 58 μm × 75 μm. The black rectangle in each image shows the location for high-resolution imaging.

technique to reveal distinct structures in the OE33 cancer cell by increasing the imaging resolution.

3.1. Whole cell IR-SNOM images

Images of the whole OE33 cancer cell are shown in figure 2. Optical microscope images have been shown [9]; a 400× image is included as figure 2(a). A topographical image of the cell is shown in figure 2(b) and figures 2(c)–(d) show the IR-SNOM images obtained at 1242 cm^{-1} in reflection and transmission modes, respectively. Images similar to figures 2(c) and (d) were obtained at each of the other four wavelengths studied [9]. The images in figure 2 are 58 μm × 75 μm with a pixel size of 1 μm. The small area marked by the black rectangles, which is entirely within the cell, was chosen for detailed investigation in this work.

A comparison of the reflection and transmission IR-SNOM images of the whole cell with their corresponding topographical image (figure 2) demonstrates that the IR-SNOM images do not simply follow the topography of the cell; a detailed analysis [9] established that while the IR-SNOM signal is influenced by topography this is not a dominant effect. The two IR-SNOM images, taken at the same wavelength, but in reflection or transmission, are very different.

There is a strong dependence of the intensity of features observed in the near-field on the vertical distance from the SNOM aperture, and as a result it is presently not possible to deduce the detailed chemical structure of the cell from a collection of two-dimensional images. As discussed earlier [9] the cell is ~2 μm thick and, although the whole thickness of the cell is in the near-field, the intensity of the signal from a chemical moiety varies as k^2/d^4 where $k = 2\pi/\lambda$, λ is the wavelength and d is the distance of the moiety from the SNOM aperture. Under the conditions of the present study, and considering only the k^2/d^4 term, it is estimated that the measured intensity from a chemical moiety reduces by almost two orders of magnitude as the molecule is located 1 μm deeper into the specimen. This simple model does not fully describe the complexity of how the signal varies but the rapid decrease in the near-field signal strength with d is a major limitation on determining the detailed chemical structure of the cell. It may be possible with a careful calibration of the instrument to obtain three-dimensional information on the chemical composition of such specimens in the future [9]. However it is possible to characterize chemical structures that have a strong contribution to the measured intensity from a chemical moiety. This is demonstrated by several examples in later sections.

The variation in the chemical composition of the cell with depth, coupled with the dependence of the evanescent wave on depth, is the most likely explanation [9] of the difference in the two-dimensional distribution of intensity of the signal observed in reflection and transmission at 1242 cm^{-1} from the nucleic acids (figures 2(c) and (d)). These images show that the nucleic acids are distributed inhomogeneously in the cell. In a normal healthy cell that is not undergoing mitosis, the DNA would be expected to reside entirely within the nucleus and the nucleus would be expected to dominate the topography. The topography together with the images from the nucleic acids indicate that the cell does not have all the characteristics of a 'normal' cell with a well-defined nucleus. The cell may have been undergoing mitosis or alternatively the abnormal topography and nucleic acid distribution may just reflect the characteristic disorder of a cancer cell. In both cases the nucleic acids may not be wholly enclosed within the nucleus.

3.2. Observation of subcellular features

To visualize the multiple chemical components within the cell a composite colour image was created by combining whole cell images (taken at a step size of 1 μm) at three wavelengths into a single image: 1242 cm^{-1}, 1370 cm^{-1} and 1538 cm^{-1} were assigned to the red, green and blue channels, respectively (figure 3(b)). If at a given pixel location the (normalized) intensities at each wavelength are similar then the pixel colour would be a dark shade of grey, as seen by the area surrounding the cell. In this image there is a clear separation of the colours, which highlights the features that occur at different wavelengths and at

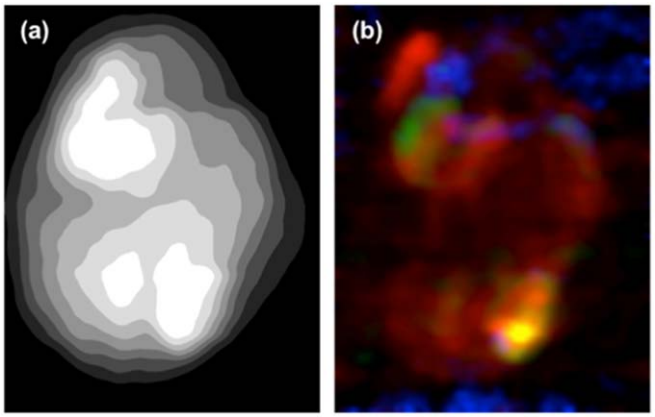

Figure 3. (a) Contour plot of the OE33 cancer cell (b) Composite colour image created by combining images taken at 1242 cm^{-1} (red), 1370 cm^{-1} (green) and 1538 cm^{-1} (blue). The images are 58 μm $\times$ 75 μm.

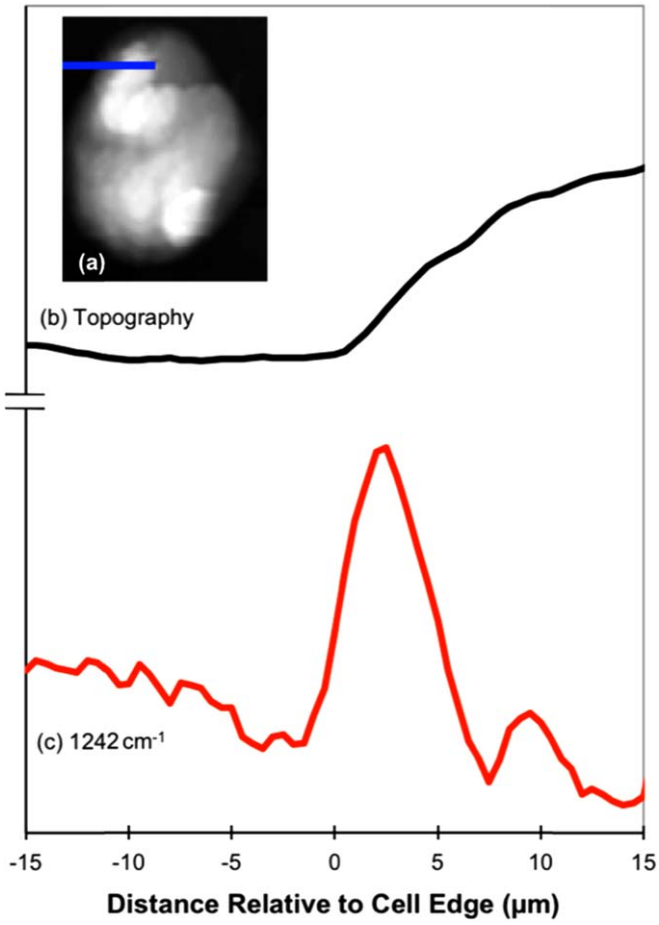

Figure 4. Line scans taken through the cell. (a) Topography image with approximate position of line scan indicated by blue line, (b) topography line scan and (c) line scan at 1242 cm^{-1}. Line scans taken through the cell are an average of five lines.

different spatial locations. In other words, those features that are strongly influenced by the chemical structure of the cell. The presence of the red colour, at various locations, further illustrates that the contribution from the nucleic acids is distributed inhomogeneously in the cell.

In order to explore the detailed chemical structure in the cell, higher-resolution line scans were obtained across the whole of the cell using a scanning step size of 0.5 μm. Figure 4 shows line scans of the higher-resolution topography and IR-SNOM obtained at 1242 cm^{-1} across the left edge of the cell. These lines were taken in a horizontal direction across the cell at the location shown by the line in the topographic image (figure 4(a)); each is an average of five line scans. The 1242 cm^{-1} line scan of the nucleic acid

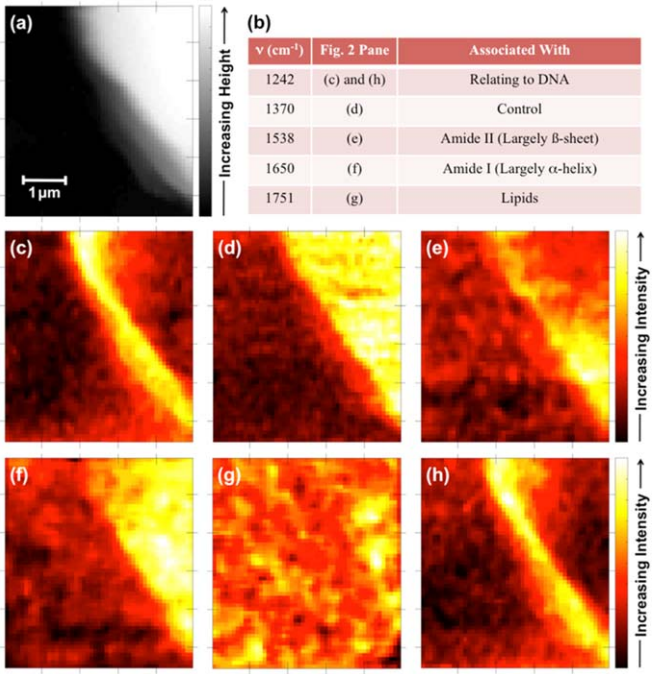

ν (cm^{-1})	Fig. 2 Pane	Associated With
1242	(c) and (h)	Relating to DNA
1370	(d)	Control
1538	(e)	Amide II (Largely ß-sheet)
1650	(f)	Amide I (Largely α-helix)
1751	(g)	Lipids

Figure 5. IR-SNOM reflection images of a 5.0 μm $\times$ 5.5 μm area of the cell. (a) Topography image with height scale bar, (b) table showing assignments of wavenumbers, (c)–(g) IR-SNOM images at 1242 cm^{-1}, 1370 cm^{-1}, 1538 cm^{-1}, 1650 cm^{-1}, 1751 cm^{-1} respectively and (h) repeat of 1242 cm^{-1}. The colour maps show increasing signal intensity from dark to light.

concentration shows an interesting feature at the edge of the cell, which clearly does not correlate with the topography. Given the <10 μm width of this feature, and its chemical composition, it is feasible that it could arise from a microvesicle about to leave the cell. Microvesicles range in size from 0.1 to 2 μm and are the focus of considerable research since they spread cancer genes [30], play a role in the metastatic spread of cancer [31], are a pathway for the suppression of the immune system [32] and offer new therapeutic opportunities [33]. Their chemical structure is of considerable interest and the strong signal from nucleic acids associated with this feature is consistent with the expected DNA or RNA composition of a microvesicle. The importance of this observation is that it demonstrates that the aperture SNOM technique has the capability to study such structures in detail.

3.3. High-Resolution IR-SNOM images

High-resolution topography and IR-SNOM reflection images of the small region of 5.0 μm $\times$ 5.5 μm, taken at the location of the black rectangle in figure 2, were obtained at five wavelengths. The raw images were processed to give the images shown in figure 5. The topography is shown in the linear grey scale image (figure 5(a)). The images shown in figures 5(c) to (h) were obtained respectively at 1242 cm^{-1}, 1370 cm^{-1}, 1538 cm^{-1}, 1650 cm^{-1}, 1751 cm^{-1} and 1242 cm^{-1}. The intensities in each light image have been separately normalized between 0 and 1 and are represented as shown in the colour bar (from dark to light with increasing signal intensity). The signal-to-noise ratio in the lipid image (figure 5(g)) is low for two reasons: firstly, at this wavelength the FEL is operating with the undulator gap at the extreme limit of its lasing range so the output is both unstable and of relatively low intensity, and secondly the lipid signal arises from a thin bilayer of molecules. The images acquired at 1242 cm^{-1} were taken at the beginning (figure 5(c)) and end (figure 5(h)) of the data collection.

Line profiles of the intensity obtained from the high-resolution images in figure 5 are shown in figure 6, where the line from which the profiles were taken is shown on the topography image (figure 6(a)). Each line profile was obtained by interpolating along multiple parallel lines adjacent to the chosen line; each point included data from a width of about 3 pixels. Each profile was then separately normalized between 0 and 1.

The most prominent feature in the IR-SNOM images in figure 5 is the intense narrow ribbon-like feature in the 1242 cm^{-1} image (figure 5(c)), which extends from the middle of the top to the bottom right and roughly coincides with an increase in the topography of the cell (figures 5(a), 6(a) and (b)). The feature has a width that varies from about 0.55 μm to 0.85 μm, which is well below the diffraction limit of the IR light. Features following the same general trend as the leading edge of the 1242 cm^{-1} feature can be observed in the other IR-SNOM images (figures 5(d)–(g) and 6(d)–(g)) but the locations of the left hand edges of these features do not coincide exactly. The finding that the SNOM signal is influenced by, but not dominated by, topography [9] is confirmed by the line

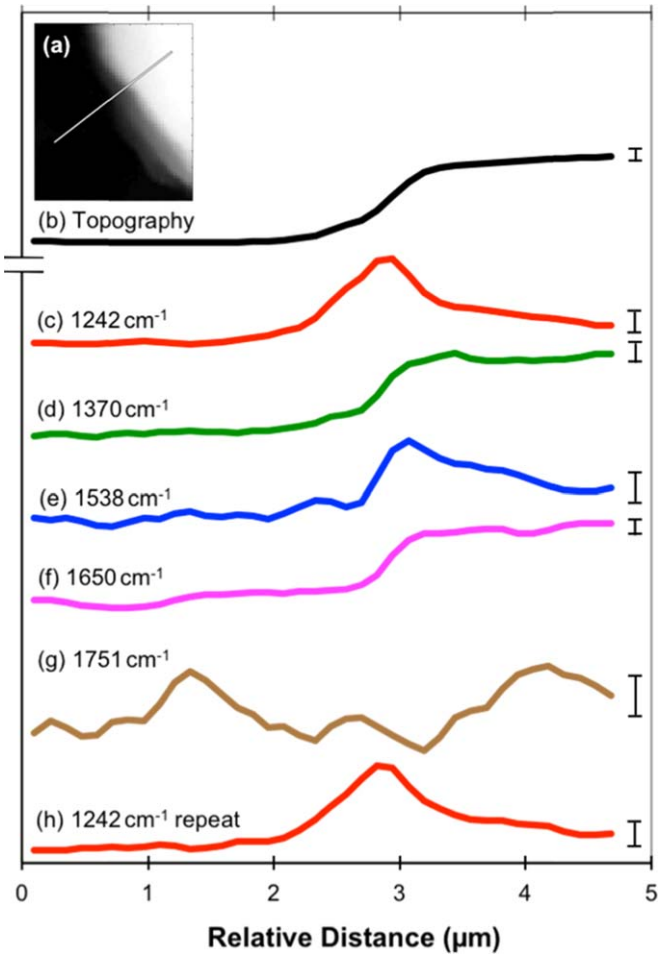

Figure 6. Line profiles taken from figure 5 showing the relationship between the spectral profiles and spatial resolution. Each line profile (b)–(h) was obtained by interpolating multiple parallel lines adjacent to the line shown in (a) from a width of about 3 pixels. The line profiles have been separately normalized between 0 and 1. Error bars (2σ) are shown to the right of each profile.

profiles shown in figure 6. Apart from the line profile observed at 1751 cm^{-1}, where the errors are relatively large, all the other profiles show a significant increase in intensity roughly in the region where the topography increases. However there are significant differences in the profiles obtained at different wavelengths and these also differ in detail from the line profile of the topography. In particular the profile obtained at 1242 cm^{-1} peaks prior to the maximum increase in topography and prior to the increase in the other three wavelengths. The profile obtained at 1538 cm^{-1} also peaks then falls away as the topography continues to increase while the profiles obtained at 1370 cm^{-1} and 1650 cm^{-1} continue to increase in line with the topography signal.

Three of the small-area high-resolution images from figure 5 have been combined into the composite colour image shown in figure 7(a). This image was formed in the same way as figure 3(b), by combining the SNOM reflection images obtained at 1242 cm^{-1}, 1370 cm^{-1} and 1538 cm^{-1} into the red, green and blue channels, respectively. The clear separation of the colours further illustrates that the features seen at the different wavelengths occur at different spatial locations. For example, the diagonal red feature shows that in this region there is relatively high intensity at 1242 cm^{-1} and low intensities at the other wavelengths. Overlaying this colour image over a surface plot of the topography (figure 7(b)) highlights the separation of chemical features seen at the different wavelengths and shows that they do not just follow the topography, as would be the case if they were only due to artefacts of scanning microscopy.

3.4. Determination of spatial resolution and reproducibility of images

IR-SNOM line profiles that exhibit abrupt changes in intensity, such as that shown in figure 6(e), can be used to estimate the spatial resolution of the technique. The distance over which the intensity changes from 20% to 80% gives a value of $0.15 \pm 0.05\ \mu$m, which is equivalent to a spatial resolution of $\sim\lambda/40$, or 20 times less than the diffraction limit. This value was obtained from the analysis of multiple profiles from different images and wavelengths. As far as the authors are aware this is the first time a cell has been imaged over such a large area with such high spatial resolution using IR radiation. The above value of $0.15 \pm 0.05\ \mu$m

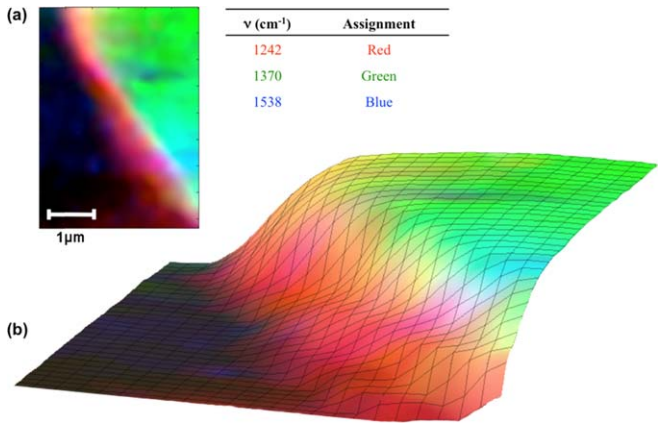

Figure 7. Alternative visualization of high-resolution IR-SNOM images. (a) Composite colour image created by combining the images (figures 5(c)–(e)) taken at 1242 cm^{-1} (red), 1370 cm^{-1} (green) and 1538 cm^{-1} (blue). (b) Overlay of the composite colour image over a surface plot of the topography (figure 5(a)). This visualization helps show that the 1242 cm^{-1} (red) and 1370 cm^{-1} (green) signals occur at different locations with respect to the topography, indicating that neither is solely an artefact of the topography.

is the spatial resolution of the high-resolution images taken with 0.1 μm step size. The diameter of the aperture of the SNOM fibre is taken to be approximately the same as the measured lateral resolution for a high-resolution image. The whole cell images, acquired with a 1 μm step size, have a spatial resolution $\approx$1 μm. For the high-resolution images, the tip was well matched to the step size with a small amount of over-sampling. However, for the whole cell images, the tip aperture was significantly smaller than the pixel size, resulting in under-sampling and a decrease in the signal-to-noise.

In order to assess the reproducibility of the results throughout the study, the first image at 1242 cm^{-1} was repeated following the acquisition of the other wavelengths for both the whole cell images and for the high-resolution images. The repeat scan for the latter is labelled as '1242 cm^{-1} repeat' and is shown as the last image and line profile [figures 5(h) and 6(h), respectively]. The two sets of data are qualitatively the same; the repeat scan shows a negligible offset of the peak maximum by about 0.1 μm.

3.5. Observation of a feature attributed to a chromosome

The narrow ribbon-like feature in figure 5(c), discussed above, was investigated further by obtaining a series of small (8 μm $\times$ 8 μm) overlapping IR-SNOM images at 1242 cm^{-1} to determine the full spatial extent of the feature. These images were pre-processed, as described above, cropped and assembled into a mosaic, which is shown in figure 8. From this image it can be seen that the feature has a definite beginning and end confirming that it is not a topographical artefact. Edge effects from surface inhomogeneities can appear as artefacts in the SNOM images and manifest themselves by an enhanced SNOM intensity that is related to a change in topography. If the ribbon-like feature did arise from an edge effect then it would follow the topography and continue beyond the top and bottom part of the image shown in figure 8.

The observations that the feature is clearly delineated only in the image obtained at 1242 cm^{-1} (which is representative of nucleic acids) and that the size of the feature is 11 μm $\times$ $\sim$0.7 μm, are both consistent with the feature being a human chromosome, which are of course predominately composed of DNA. Further evidence would be required to confirm the exact identity of the observed feature. However, the result is important because it is the first demonstration of the ability of the IR-SNOM technique to chemically image features consistent with a human chromosome in a cancer cell. The authors know of no chemical technique that could identify the chemical composition of such a feature inside a cell with the same or better spatial resolution. The observation of this feature establishes the potential to study chromosome abnormalities that give rise to a large number of human diseases [34]. They also play a fundamental role in many cancers [35, 36] including inducing the important, but little understood, transformation of epithelial cells to mesenchymal cells that lead to metastasis [37]. Furthermore, given the spatial extent of the feature and the cell within which it was located, it would be difficult to study in the IR with any other technique.

4. Conclusions

The combination of an IR-SNOM, with an imaging tip of aperture diameter $\sim$0.1 μm, and the tuneable ALICE IR-FEL has been shown to yield excellent images of dimensions 5.0 μm $\times$ 5.5 μm with a spatial

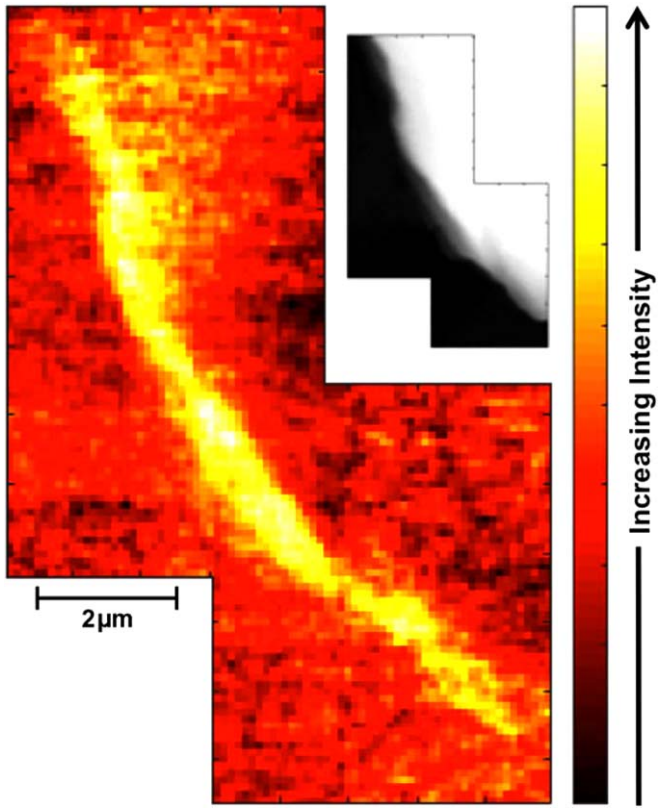

Figure 8. Mosaic of three 1242 cm^{-1} IR-SNOM images to show the feature attributed to a chromosome which has an overall finite length of 11 μm. The insert shows the corresponding topography image.

resolution of 0.15 $\pm$ 0.05 μm. Tuning of the IR-FEL radiation to the wavelengths of particular biomarkers has revealed chemically differentiated subcellular structures in a human oesophageal adenocarcinoma cell. Signals from the topography, IR-SNOM, and IR-reference were collected simultaneously, making it possible to relate the topography of the cell to its chemical structure. The general topographic and chemical structure of the cell indicate that the cell may have undergone mitosis or alternatively showed the disorder that is characteristic of cancer cells. An advantage of the technique is that high spatial resolution ($\sim\lambda/40$) can be obtained over a wide range of areas and IR wavelengths thus yielding information on the chemical structure of the specimen. These advantages would clearly apply to other areas of research including soft condensed matter, solid state materials and biological studies.

The technique has yielded the first IR observation of a feature that is consistent with a human chromosome in a cancer cell and has a unique capability to locate and study the physical and chemical structure of such features. Chromosome abnormalities are a feature of a large number of human diseases [34]. They also play a fundamental role in many cancers [35, 36] including inducing the important, but little understood, transformation of epithelial cells to mesenchymal cells that lead to metastasis [37].

The aperture SNOM technique has also been shown to have the capability of studying the physical and chemical structure of a feature that is consistent with microvesicles. Microvesicles are the focus of considerable research since they spread cancer genes [30], play a role in the metastatic spread of cancer [31], are a pathway for the suppression of the immune system [32] and offer new therapeutic opportunities [33].

Acknowledgments

This work was supported by the UK Engineering and Physical Sciences Research Council (UK EPSRC: Grant No. EP/K023349/1). JI and TC acknowledge support from EPSRC studentships. The authors acknowledge and express thanks to the following: All ASTeC staff who were key commissioners running ALICE and Daresbury staff who provided endless support; Prof. George King, University of Manchester for his help, support and for acting as a second commissioner and Dr Chris Edmonds, Cockcroft Institute for acting as a second commissioner.

ORCID iDs

C I Smith https://orcid.org/0000-0001-6878-0697
P Weightman https://orcid.org/0000-0002-0907-3930

M R F Siggel-King https://orcid.org/0000-0002-0547-3670

References

[1] Lippincott-Schwartz J and Patterson G H 2009 *Trends Cell Biol.* **19** 555
[2] Fernández-Suárez M and Ting A Y 2008 *Nat. Rev. Mol. Cell Biol.* **9** 929
[3] Gardner P 2016 *Advanced Vibrational Spectroscopy for Biomedical Applications Faraday Discuss.* vol 187(Cambridge, UK, 21–23 March 2016) ed P Gardner (RSC: Cambridge) and references therein
[4] Baker M J, Gazi E, Brown M D, Shanks J H, Clarke N W and Gardner P 2009 *J. Biophoton.* **2** 104
[5] Smith A D *et al* 2013 *App. Phys. Lett.* **102** 053701
[6] Halliwell D E *et al* 2016 *Sci. Rep.* **6** 29494
[7] Cricenti A, Generosi R, Luce M, Perfetti P, Margaritondo G, Talley D, Sanghera J S, Aggarwal I D and Tolk N H 2002 *Phys. Chem. Chem. Phys.* **4** 2738
[8] Craig T *et al* 2018 *Phys. Status Solidi B* 1700518
[9] Ingham J *et al* 2018 *Biomed. Phys. Eng. Express* **4** 025011
[10] Knoll B and Keilmann F 1999 *Nature* **399** 134
[11] Kazantsev D V and Ryssel H 2013 *Appl. Phys. A* **113** 27
[12] Yoxall E, Navarro-Cia M, Rahmani M, Maier S A and Phillips C C 2013 *Appl. Phys. Lett.* **103** 213110
[13] Dazzi A, Prazeres R, Glotin F and Ortega J M 2005 *Opt. Lett.* **30** 2388
[14] Donaldson P M, Kelly C S, Frogley M D, Filik J, Wehbe K and Cinque G 2016 *Opt. Express* **24** 1852
[15] Amrania H, Drummond L, Coombes R C, Shousha S, Woodley-Barker L, Weir K, Hart W, Cartera I and Phillips C C 2016 *Faraday Discuss.* **187** 539
[16] Hermann P, Hoehl A, Patoka P, Huth F, Rühl E and Ulm G 2013 *Opt. Express* **21** 2913
[17] Bechtel H A, Muller E A, Olmon R L, Martina M C and Raschk M B 2014 *Proc. Nat. Acad. Sci.* **111** 7191
[18] Chen X, Lo C F B, Zheng W, Hu H, Dai Q and Liu M 2017 *Appl. Phys. Lett.* **111** 223110
[19] (https://anasysinstruments.com/technlogy/nanoir-technology/) (accessed on 11-07-2018)
[20] Thompson N R, Dunning D J, Clarke J A, Surman M, Smith A D, Saveliev Y and Leonard S 2012 *Nucl. Instrum. Methods Phys. Res. A* **680** 117
[21] Thompson N R *et al* 2015 Status of the ALICE IR-FEL: from ERL demonstrator to user facility *Int. Free Electron Laser Conf. - FEL 2015* ed H S Kang, D-E Kim and V R W Schaa pp 379–83
[22] Unger M A, Kossakovski D A, Kongovi R, Beauchamp J L, Baldeschwieler J D and Palanker D V 1998 *Rev. Sci. Instrum.* **69** 2988
[23] Rockett J C, Larkin K, Darnton S J, Morris A G and Matthews H R 1997 *Brit. J. Cancer* **75** 258
[24] Susi H and Byler D M 1986 *Methods Enzymol.* **130** 290
[25] Maiti N C, Apetri M M, Zagorski M G, Carey P R and Anderson V E 2004 *J. Am. Chem. Soc.* **126** 2399
[26] Movasaghi Z, Rehman S and ur Rehman I 2008 *Appl. Spectrosc. Rev.* **43** 134
[27] Bellisola G and Sorio C 2012 *Am. J. Cancer Res.* **2** 1
[28] Talari A C S, Martinez M A G, Movasaghi Z, Rehman S and ur Rehman I 2017 *Appl. Spectrosc. Rev.* **52** 456
[29] Zucchiatti P, Mitri E, Kenig S, Bille F, Kourousias G, Bedolla D E and Vaccari L 2016 *Anal. Chem.* **88** 12090
[30] Rak J and Guha A 2012 *Bioessays* **34** 489
[31] Asfar A S, Bao B and Sarkar F H 2013 *Cancer Metast. Rev.* **32** 623
[32] Zhang H G and Grizzel W E 2011 *Clin. Cancer Res.* **17** 959
[33] Andaloussi S E L, Mäger I, Breakefield X O and Wood M J A 2013 *Nat. Rev. Drug Discov.* **12** 347
[34] Theisen A and Shaffer L G 2010 *Appl. Clin. Genet.* **3** 159
[35] Rowley J D 1980 *Cancer Genet. Cytogen.* **2** 175
[36] Fröhling S and Döhner H 2008 *N. Engl. J. Med.* **359** 722
[37] Gao C, Su Y, Koeman J, Haak E, Dykema K, Essenberg C, Hudson E, Petillo D, Khoo S K and Vande Woude G F 2016 *Proc. Nat. Acad. Sci.* **113** 14793